

Momentum Distribution Spectroscopy Using Deep Inelastic Neutron Scattering

G.F.Reiter

Physics Department, University of Houston

J. Mayers

Rutherford -Appleton Laboratory, Didcot, England

J. Noreland

Defence Research Establishment, Sweden

We show that deep inelastic neutron scattering from hydrogen(or other light nuclei) can be used to measure a spectrum of anharmonic contributions to the target atom momentum distribution with high and known accuracy . The method is applied here to determine the momentum distribution of the hydrogen in the hydrogen bonded system KHC_2O_4 (potassium binoxalate), where 13 anharmonic coefficients are obtained at the 2σ to 3σ level. The momentum distribution is obtained to an accuracy of better than few percent at all significant values of momentum.

I. INTRODUCTION

The measurement of proton momentum distributions by neutron scattering is analogous to the measurement of electron momentum distributions by Compton scattering [1] and measurement of nucleon momenta by Deep Inelastic Scattering [2] and is known as Neutron Compton Scattering (NCS) or Deep Inelastic Neutron Scattering (DINS). All three techniques rely upon the fact that if the momentum transferred from the incident to target particle is sufficiently large, the impulse approximation (IA) can be used to interpret the data. In the IA, momentum and kinetic energy are conserved. From a measurement of the momentum and energy change of the neutron, the momentum of the target nucleus before the collision can be determined.

DINS measurements have only become practical since the construction of intense accelerator based neutron sources, which have allowed inelastic neutron scattering measurements with energy transfers in the eV region [3]. Energy transfers much greater than the maximum vibrational frequency of the target atom are required before the IA can be used to reliably determine the momentum distribution . At lower energy transfers the IA is no longer valid and is not related in a simple way to the observed scattering intensities.

There have been a few pioneering studies on anisotropic systems at eV energy transfers [4–8] but the analysis has been limited to fitting Gaussians to the observed data, or more generally fitting the data with model containing a few parameters, as was done for measurements on molecular hydrogen [9]. We show here that an entire spectrum of anharmonic coefficients can be measured without recourse to any model, in addition to the widths of an anisotropic gaussian, thus describing an arbitrary anisotropic and anharmonic momentum distribution, The possibility of doing this for isotropic systems was first suggested by Reiter and Silver, [10] That possibility, for more general systems, is now a reality. We demonstrate this by measuring the momentum distribution for KHC_2O_4 where we obtain 14 anharmonic coefficients whose size varies by nearly two orders of magnitude, with at least $2\text{--}3\sigma$ confidence levels for all but one. The experimental instrument is the EVS spectrometer at ISIS. The work presented here by no means represents the limits of resolution of the instrument, but rather the first experiments of this kind. Upgrades are planned in the near future that will significantly increase flux and counting efficiency.

THEORY OF MEASUREMENT

The theoretical basis of neutron Compton scattering is the impulse approximation (IA), which is exact when the momentum transfer and energy transfer are infinite [11–13]. The neutron scattering function $S(\vec{q}, \omega)$, is related to the momentum distribution $n(\vec{p})$ in the impulse approximation limit by the relation

$$S(\vec{q}, \omega) = \frac{M}{q} \int n(\vec{p}) \delta(y - \vec{p} \cdot \hat{q}) d\vec{p} = \frac{M}{q} J(\hat{q}, y) \quad (1)$$

where $y = \frac{M}{q}(\omega - \frac{q^2}{2M})$, M is the mass of the target particle, $q = |\vec{q}|$, and $\hat{q} = \vec{q}/q$.

DINS measurements on protons have a particularly simple interpretation, as the interaction of protons with other atoms can usually be accurately accounted for [14–16] in terms of a single particle potential and hence by a proton

wave function. [17] From elementary quantum mechanics, $n(\vec{p})$ is related to the Fourier transform of the proton wave function via,

$$n(\vec{p}) = \frac{1}{(2\pi)^3} \left| \int \Psi(r) \exp(ip \cdot \vec{r}) d\vec{r} \right|^2 \quad (2)$$

and a DINS measurement of $n(\vec{p})$ can be used to determine the wave function in an analogous way to the determination of real space structure from a diffraction pattern. If $n(\vec{p})$ is known, and if the proton is in a site with reflection symmetry, so that the wave function can be assumed real, then in principle both the proton wave function and the exact form of the potential energy well in which the proton sits can be directly reconstructed. [10] With an asymmetric site such as potassium binoxalate, the phase information that is lost by taking the absolute value of the momentum wavefunction is irrecoverable, and we will not be able to reconstruct the potential directly. The $n(\vec{p})$ obtained can, of course, be used to check any model potential.

While the original formulation of the inversion problem [10] is complete as it stands, it is useful for the systems we will be dealing with to take into account the anisotropy of the system explicitly. The fundamental result that allows for a simple inversion of the Radon transform, $J(\hat{q}, y)$ to obtain $n(\vec{p})$ makes use of a basis of Hermite polynomials and spherical harmonics in which the transform is diagonal. That is, a single term in the series for $J(\hat{q}, y)$ corresponds to a single term in the expansion of $n(\vec{p})$.

If we express $J(\hat{q}, y)$ in this basis as

$$J(\hat{q}, y) = \frac{e^{-y^2}}{\pi^{\frac{1}{2}}} \sum_{n,l,m} a_{n,l,m} H_{2n+l}(y) Y_{lm}(\hat{q}) \quad (3)$$

then $n(\vec{p})$ is given in the related basis of Laguerre polynomials as

$$n(\vec{p}) = \frac{e^{-p^2}}{\pi^{\frac{3}{2}}} \sum_{n,l,m} 2^{2n+l} n! (-1)^n a_{n,l,m} p^l L_n^{l+\frac{1}{2}}(p^2) Y_{lm}(\hat{p}) \quad (4)$$

where \hat{p} and \hat{q} are unit vectors. Clearly, since the expansions are complete, a distribution of the form

$$n(\vec{p}) = \prod_i \frac{e^{-\frac{p_i^2}{2\sigma_i^2}}}{(2\pi\sigma_i)^{\frac{1}{2}}} R(\vec{p}) \quad (5)$$

with the σ_i significantly different from each other, could be expanded in this form, but even if $R(\vec{p})$ were 1, it would require a large number of terms in the series. To avoid this, we show that the anisotropy may be taken into account by a change of variables, so that the coefficients $a_{n,l,m}$ represent genuinely anharmonic contributions.

Introducing the new variables

$$p'_i = p_i / \sqrt{2}\sigma_i \quad (6)$$

with $n(\vec{p})$ defined as in Eq. (5), defining $R'(\vec{p}') = R(\vec{p}(\vec{p}'))$ and

$$n'(\vec{p}') = \frac{e^{-p'^2}}{\pi^{\frac{3}{2}}} R'(\vec{p}') \quad (7)$$

we have

$$J(\vec{q}, y) = \int n'(\vec{p}') \delta(y - \vec{p}' \cdot \vec{q}') d\vec{p}' \quad (8)$$

where $q'_i = q_i \sqrt{2}\sigma_i$. The right hand side of Eq. (8) is no longer a Radon transform, since \vec{q}' is not a unit vector. However, defining $y' = y/|\vec{q}'|$ we obtain

$$J(\vec{q}, y) = \frac{1}{|\vec{q}'|} \int n'(\vec{p}') \delta(y' - \vec{p}' \cdot \hat{q}') d\vec{p}' = \frac{1}{|\vec{q}'|} J'(\hat{q}', y') \quad (9)$$

where $J'(\hat{q}', y')$ is the Radon transform of the isotropic (in its gaussian component) but anharmonic distribution $n'(\vec{p}')$. If \hat{q} is specified as a unit vector in the usual spherical coordinates, then

$$|\vec{q}'| = \sqrt{2}((\sigma_1 \sin(\theta) \cos(\phi))^2 + (\sigma_2 \sin(\theta) \sin(\phi))^2 + (\sigma_3 \cos(\theta))^2)^{\frac{1}{2}} \quad (10)$$

Our procedure is to expand $J'(\hat{q}', y')$ in hermite polynomials, as in Eq. (3), and least squares fit the data, $S(\vec{q}, \omega)$, using Eqs. (1,9,10), to obtain the parameters, $\sigma_i, a_{n,l,m}$. $n'(\vec{p}')$ can then be reconstructed as in Eq. (4), and we thus obtain $n(\vec{p})$ as in Eq.(5) with $R(\vec{p}) = R'(\vec{p}'(\vec{p}))$. That this is a practical procedure will be demonstrated below.

II. MEASUREMENTS

The measurements were performed on the electron volt spectrometer eVS [18] at the ISIS neutron source. On EVS the energy of the scattered neutron is fixed by a resonance filter difference technique [19]. The final neutron velocity and energy are related by $E_1 = m\nu_1^2/2$ where m is the neutron mass. The energy of the incident neutron is determined from a measurement of the neutron time of flight via the equation

$$t = \frac{L_0}{\nu_0} + \frac{L_1}{\nu_1} \quad (11)$$

where t is the measured time of flight, L_0 and L_1 are the lengths of the incident and the scattered flight paths of the neutron, ν_0 and ν_1 are the speeds of the incident and scattered neutrons. Then

$$\omega = m(\nu_0^2 - \nu_1^2)/2 \quad (12)$$

and

$$q = m(\nu_0^2 + \nu_1^2 + 2\nu_1\nu_0 \cos\theta)^{\frac{1}{2}} \quad (13)$$

where θ is the scattering angle. From these equations ω and \vec{q} can be determined for a given time of flight t , if the instrumental parameters L_0, L_1, θ and E_1 are known. Hence from the count rate at a given time t , $J(\hat{q}, y)$ can be determined. On eVS the detectors are situated in the horizontal plane and hence \vec{q} is always horizontal. By orienting the sample with a chosen crystal axis vertical, it is possible to measure $J(\hat{q}, y)$ for \vec{q} in whichever plane, relative to the sample, one chooses. A time of flight scan at a particular angle for a given detector does not correspond, however, to a particular direction of \vec{q} . There is significant curvature of this scan through the proton momentum space since the direction of \vec{q} varies significantly over the data region. Time of flight spectra for eight adjacent detectors at angles between 35 and 55 degrees scan through the atomic momentum momentum space of the proton as illustrated in figure 1

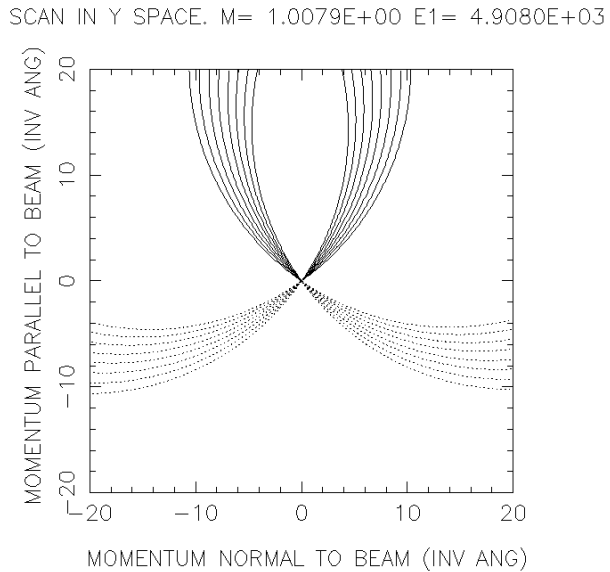


FIG. 1. Scan pattern in momentum space for detectors at a fixed angle as the time of flight is varied

A complete scan over the proton momentum space is constructed by combining a number of data sets, taken with the sample rotated about the vertical axis by appropriately chosen angles.

The reported measurements were made using two banks of 8 Li^6 doped glass scintillator detectors which were symmetrically placed on each side of the incident beam at scattering angles between 35° and 55° . For DINS studies of protons it is necessary to site the detectors at forward scattering angles since the hydrogen scattering cross section is strongly anisotropic at eV incident energies, with virtually no back scattering. This restriction is a kinematic consequence of the closeness of the mass of the neutron and the hydrogen atom and does not apply to heavier atoms.

The resolution function of the instrument is determined by the uncertainties in the measured values of the time of flight t and the distribution of L_0, L_1, θ and E_1 values allowed by the instrumental geometry and analyser foil resolution. Uncertainties in L_0 arise primarily from the finite depth of the neutron moderator, those in L_1 and θ from the finite sample and detector sizes and those in t from jitter in the detector electronics. All resolution components can be determined by calibration measurements and all except the energy component can be approximated by Gaussians, without significant error. A 0.015 mm thick gold foil provided a Lorentzian energy resolution function at $E_1 = 4908\text{ meV}$, with a peak HWHM of 136 meV. The Gaussian and Lorentzian resolution components in momentum space y , are listed in table 1 for two angles representative of the range of angles employed. The resolution is dominated by the energy component which varies strongly with scattering angle. The second most important contribution comes from the angular resolution of the spectrometer and is independent of angle. The momentum and energy transfers at the centre of the hydrogen response peak are also listed for the different angles.

Table 1. The resolution widths are the Lorentzian HWHM for (RL) and the Gaussian standard deviation for other parameters (RG) . The momentum q and energy transfer (at the scattering angles 35° and 55° are also given.)

Angle	$R_G(\text{\AA}^{-1})$	$R_L(\text{\AA}^{-1})$	$q(\text{\AA}^{-1})$	$\omega(\text{eV})$
35°	0.61	1.08	34.1	2.41
55°	0.55	0.55	48.8	4.92

The raw data contains signals from all the atoms in the scattering sample and from the cryostat background. Fortunately the energy transfer to hydrogen is much greater than that to other atomic masses and the proton signal is well separated from that due to other masses. The contribution from all components other than hydrogen is subtracted by fitting a sum of Gaussians convoluted with the instrument resolution function to the data and subtracting off the fitted contribution to other peaks. There is also a small contribution to the data from a second gold resonance at 60 eV which can be seen at 100 \mu sec and this is also fitted and subtracted from the data.

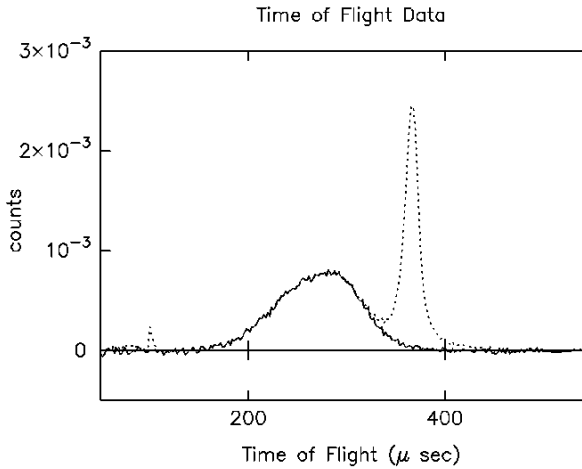


FIG. 2. The sum of data from 8 detectors at scattering angles between 38° and 55° is shown as the dotted line. The data after subtraction of the contribution from atoms with higher masses and the 60 eV resonance data is shown as the full line. The total data set for a single plane consisted of 36 such spectra. The FWHM of the Lorentzian resolution function is 6 microsec.

The data for each scan was converted into a distribution in the momentum space of the crystal as described above. Complete coverage of the plane was achieved by combining six runs which were taken at steps of 23° sample rotation.

A contour plot of the data derived from the six runs is shown in figure 3. This was produced by binning the counts from different detectors and sample orientations in the appropriate pixel of the momentum space

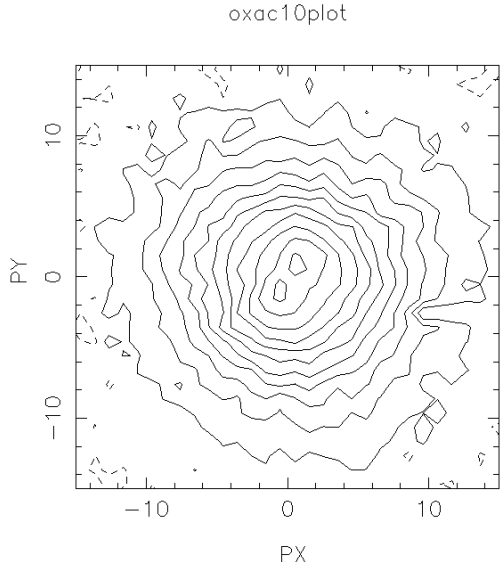


FIG. 3. Contour plot of data in one plane of potassium binoxalate. The apparent double peak near the origin is an artifact of the method of plotting the data

The data has been corrected for sample attenuation, but still contains errors due to small deviations from the Impulse Approximation which are present at the finite momentum transfers of the measurement. These tend to introduce small asymmetries into the data set at the 1-5% level, thereby removing the exact inversion symmetry of the Compton profile. It has been shown by Sears [20] that most of these effects are removed by symmetrisation of the data about the origin. This procedure cannot be followed for our data sets as the scan in a single detector is curved and different points in the crystal plane which are related by inversion symmetry may have been measured in different detectors, with different experimental resolution. However by fitting to a $J(\vec{q}, y)$ with inversion symmetry, as discussed below, we automatically include a correction for deviations from the impulse approximation. Any asymmetries are ignored by the fit and should not affect the values of the fitted parameters.

III. FITTING PROCEDURES

Eqs.(3,4) hold quite generally for Radon transform pairs, but physical requirements in the present context restrict the allowed coefficients. Since $J(\vec{q}, y)$ is an even function of y , l is restricted to even values, and since $J(\vec{q}, y)$ is real, the $a_{n,l,m}$ for $\pm m$ must be equal. In fact, if there are residual final state effects in the data, the data will not be symmetric. Restricting the coefficients in this way will therefore eliminate these residual effects. Lifting the restrictions and fitting the data allows one to measure the extent of these effects. For potassium binoxalate, data was taken for three perpendicular planes oriented parallel to the crystal axes. The procedure followed was to perform a simultaneous fit to the $6 \times 16 \times 3 = 288$ separate time of flight spectra to an expansion of the form given in Eq.(3), convoluted with the instrument resolution function

The actual fitting procedure requires that three of the parameters $\sigma_i, a_{n,l,m}$ be fixed, as they are not all independent. That is, if one varies the σ_i arbitrarily, there will always be a set of $a_{n,l,m}$ that will fit the data, the particular values that fit depending on the choice of the σ_i . One could obtain fixed values for the σ_i by first fitting the data to a gaussian, i.e. $R'(\vec{p}') = 1$, and then varying only the $a_{n,l,m}$, in which case all such terms would in principle be needed. We find in practice, that better results are obtained, i.e. fewer anharmonic coefficients needed and more rapid convergence of the series for $R'(\vec{p}')$, when the σ_i are allowed to vary but the first three anharmonic coefficients, $a_{1,0,0}, a_{0,2,0}, a_{0,2,2}$ are set to zero. In fact, these coefficients are not really anharmonic coefficients at all. They could always be eliminated by a shift of the σ_i and an adjustment of higher order coefficients. This procedure thus has the virtue as well of producing only genuinely anharmonic corrections to a gaussian fit.

The datasets as they are presently obtained in the EVS spectrometer at ISIS, are obtained one plane at a time (see discussion of experimental apparatus). That is \vec{q} varies within a plane, and a range of y values is taken such that

$J(\vec{q}, y)$ is negligible outside this range. There is a very high density of points, which for the purposes of the present discussion we can take to be continuous. The question then arises, 'How many planes of data are needed to determine a specified number of coefficients, and at what angles to each other should they be?' We can see the point of the question by considering first a single plane and looking at the fit to the leading anharmonic coefficient. From Eq.(3) we see that there are six independent coefficients multiplying H_4 , i.e. the coefficients of $(Y_{00}, Y_{20}, Y_{22}, Y_{40}, Y_{42}, Y_{44})$. Let us say that our coordinate system is chosen so that the plane measured is treated as an xz plane. Then in terms of the variable θ there are only three independent fourier coefficients that can be present in the data for the coefficients of H_4 , i.e. the coefficients of $(1, \cos(2\theta), \cos(4\theta))$ for instance. Therefore three of the coefficients are not independent. The complete set of coefficients cannot be determined by the data. This is of course due to the fact that there is no information as to the behaviour of $J(\vec{q}, y)$ for nonzero azimuthal angles ϕ in the data, so we shouldn't expect the fitting procedure to provide it. The data provides a complete description of $J(\vec{q}, y)$ only if this function is rotationally invariant about the z axis. Actually, what is required is only that $J'(\vec{q}', y')$ be rotationally invariant, since the fit is done in the primed coordinate system. If this is the case, then all coefficients of Y_{lm} with non-zero values of m must be zero. We see that there are only three remaining possibly non zero coefficients, which can all be determined. For higher order terms as well, keeping only the coefficients with $m=0$ provides all the independent terms needed to fit the data, and the resulting fit, of course, is rotationally symmetric about the z axis.

If the data is not known to be rotationally symmetric, additional planes of data must be taken to determine even these lowest order coefficients. In general, whenever we take another plane of data, we might expect to obtain 3 more independent measurements of the coefficients of H_4 , 4 independent measurements of the coefficients of H_6 , and in general, $k+1$ measurements of the coefficients of H_{2k} . ($k+1$ being the number of independent fourier components in the data for that value of k). Since the number of $a_{n,l,m}$ that are to be determined for $2n+l=2k$ is $(k+2)(k+1)/2$, it appears that $(k+2)/2$ planes are needed to measure all coefficients up to H_{2k} . The angles between the planes must be chosen, however, so that the measurements are really independent. For instance, if $k=2$, it would appear that two planes would suffice, but if they are chosen as the xz and yz planes, they do not provide independent measurements of the coefficients. This may be seen by observing that the sum of the data from the two planes gives three independent fourier coefficients to determine four independent $a_{n,l,m}$, the coefficients of $(Y_{00}, Y_{20}, Y_{40}, Y_{44})$, since the coefficients of Y_{22} and Y_{42} cannot affect this sum. The difference of the data on the two planes gives three equations for the two coefficients of Y_{22} and Y_{42} . A better choice for the planes would be $\phi = 0$ and $\phi = \pi/4$, which would allow the determination of all the coefficients. If there is some symmetry in the problem, one may be able to use perpendicular planes if the symmetry axis is chosen appropriately with respect to the common axis of the two scattering planes. For instance, if there is tetragonal symmetry present, and the symmetry axis is chosen perpendicular to the common axis, one can obtain all the allowed coefficients up to $k=4$. One can show that three perpendicular planes do in fact suffice to determine the coefficients up to $k=4$ in the general case, without any symmetry to reduce the number of allowed coefficients. The question of whether this is an optimum configuration of planes or not, we will leave to another time. Including the three σ_i , a three plane measurement allows 34 coefficients to be measured.

IV. MEASUREMENT ERRORS

The uncertainty in the measurement of $n(\vec{p})$ at some point \vec{p} is due to the uncertainty in the measured coefficients. Denoting an arbitrary coefficient by ρ_i , we have

$$\delta n(\vec{p}) = \sum_i \frac{\delta n(\vec{p})}{\delta \rho_i} \delta \rho_i \quad (14)$$

The fitting program, after a minimum is obtained with some set of coefficients, calculates the correlation matrix $\langle \delta \rho_i \delta \rho_j \rangle$ by varying the coefficients slightly and calculating the curvature of the chi-square of the fit. [21]. Hence, the variance in the momentum distribution is

$$\langle \delta n(\vec{p})^2 \rangle = \sum_{i,j} \frac{\delta n(\vec{p})}{\delta \rho_i} \frac{\delta n(\vec{p})}{\delta \rho_j} \langle \delta \rho_i \delta \rho_j \rangle \quad (15)$$

There are of course, potential systematic errors that could enter the measurement, such as multiple scattering effects, or an error in determining the resolution function. The former must be handled with good experimental design, and if small, can be corrected for. We have done measurements on samples whose thickness differed by a factor of two, with no significant differences in the observed scattering. Multiple scattering effects would also lead to asymmetries in $J(\vec{q}, y)$ that are not observed. The resolution function has been studied extensively, and is believed to be known

accurately. In the present measurement, the resolution width is between 15 and 25% of the width of the distribution measured.

A further source of error not contained in the estimate in Eq.(15) is the truncation of the series used to fit the data to include only terms up to $2n+l=8$. To get an idea of the seriousness of this, and to test the fitting procedures and software, we have generated synthetic data from a known momentum distribution that corresponds to an asymmetric double well, and convolved it with the instrumental resolution function. The data was then analyzed by the means described above, and the extracted $n(\vec{p})$ compared with the input. The input $n(\vec{p})$ corresponded to a spatial wave function consisting of two displaced gaussians with the same variance and a relative weight $r=.5$. The explicit form is

$$n(p_x, p_y, p_z) = \frac{(1 + r^2 + 2r\cos(2p_z a))}{(1 + r^2 + 2r e^{-\frac{a^2}{2\sigma_z^2}})} \prod_i \frac{e^{-\frac{p_i^2}{2\sigma_i^2}}}{(2\pi\sigma_i)^{\frac{1}{2}}} \quad (16)$$

where $\sigma_x = 4.6$, $\sigma_y = 4.0$, $\sigma_z = 6.0$ and $a=.15$ in units of inverse angstroms and angstroms, respectively. This form is rather similar to the actual form of the data we will analyze. The coordinate system z axis was chosen to be identical with the crystal z axis. The comparison is shown in fig 4. The extracted $n(\vec{p})$ is plotted with a dotted line, the input $n(\vec{p})$ above with a dashed line. As may be seen from the figure, there is essentially no error due to the truncation of the the expansion. Of course, an input with more variation might require including higher terms in the expansion, and hence taking more planes of data. The actual data we have obtained for potassium binoxalate has less variation than the simulation and the truncation error will be negligible. In the other directions, the fit is rigorously gaussian, since all coefficients with $m \neq 0$ were zero. We note that the measured σ_z parameter was 4.47, not 6.0. It is simply a fitting parameter. The overall momentum distribution has physical significance, the individual parameters may not. In fact, we have gotten the same degree of fit with the crystal z axis aligned along the coordinate y axis. In this case, all the coefficients are non-zero, but the resultant $n(\vec{p})$ is identical to the one displayed above.

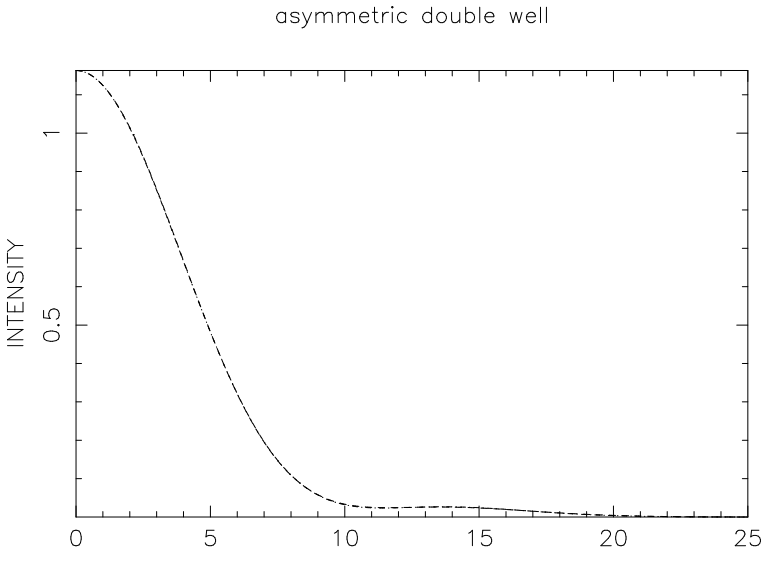


FIG. 4. Comparison of input $n(\vec{p})$, given by Eq.(16) with reconstruction of $n(\vec{p})$ using fitting procedure. The z coordinate axis is chosen to be the double well axis.

A final source of systematic error involves the possibility of finding a false minimum with the fitting procedure. With such a large number of parameters, there is the possibility that the program will home in on a local minimum and miss the true minimum. We are using straightforward gradient methods for the search, which would have difficulty with a very rugged chi-squared landscape. We do not appear to have such a landscape for these problems, and certainly not for the large parameters, such as the σ_i , or the largest anharmonic coefficients, whose values appear to be quite robust with regards to different paths to the minimum. One can check for this problem by orienting the fitting coordinate system differently with respect to the crystal axes, as was done for the test data above. In this case, all the coefficients will be different, but the final $n(\vec{p})$ must be the same. There is also the fact that $n(\vec{p})$ must be positive, and a spurious fit that leads to significant negative values can be rejected. We can also eliminate some parameters which are consistently much smaller than their variance, and which can be set to zero without affecting

significantly the chi-square, thus reducing the dimensionality of the space. We believe there are no problems of this sort with the fits we will present.

V. RESULTS FOR POTASSIUM BINOXALATE

Potassium Binoxalate, KHC_2O_4 , is a hydrogen bonded system in which the hydrogen sits in an asymmetric position between two oxygen atoms. [22]. The crystal is monoclinic. We will choose a primitive cell for which the bond axis, that is the line joining the two oxygen atoms, is essentially aligned with the c axis of the crystal. [23] We choose this axis for the z axis of our coordinate system. Three planes of data were taken at right angles to each other, with 69,632 data points in all. One of these is the bc plane, where the b axis is the unique axis, and the other two are the a^*b and a^*c plane, where the a^* axis is perpendicular to the bc plane. These were fit with the methods described above to give the momentum distribution. The measurements were done at 10 deg K and hence there are no significant finite temperature corrections to the ground state momentum distribution due to excited states.

Note that the coordinate system used to describe the momentum distribution need not have the symmetry of the crystal. The local symmetry of the site is only a two-fold rotation. We show the values of the fitted coefficients in tables 2 and 3, along with the rms uncertainty in their values. This is included only to give some sense of the individual parameter. The error in $n(\vec{p})$ is given by Eq.(14) and includes the effect of the correlations between coefficients, whereas the figures cited in the table are only the diagonal correlation coefficients. It can be seen, that many of the measured coefficients have been determined at the 2-3 σ level of confidence, some at higher levels, and only one at a 1σ level. Coefficients that are set to zero in the fitting procedure were found to have values smaller than their variance by at least a factor of 2, and setting them to zero did not significantly change the minimum value of chi-square. The goodness of fit to a sample of the data is shown in Fig. 5.

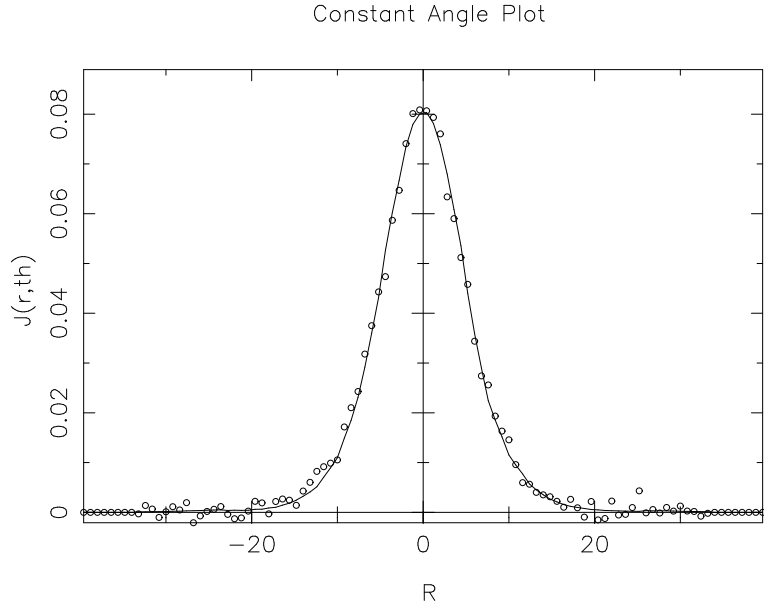


FIG. 5. Data fitted by method described above. The data is a composite of data points in a 10deg wedge about the z axis.

We have compared the fitted prediction, convolved with the instrumental resolution, and the data, for the cumulative sum of data in a 10 degree wedge along the hydrogen bond direction. The measured momentum distribution along the axes of the measurement planes, are shown in Figs. 6-9, and contour plots along coordinate planes in Figs. 10-13.

potassium binoxalate

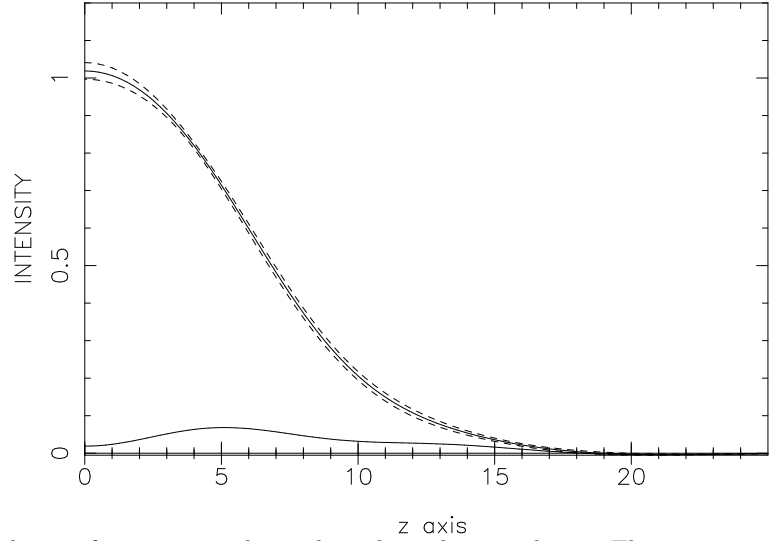


FIG. 6. Momentum distribution for potassium binoxalate along the axis shown. The momentum is in units of \AA^{-1} , $n(\vec{p})$ is in arbitrary units. The errors are calculated as in Eq.(15) for the parameters that are significant in Tables 2 and 3. The lower curve is the anharmonic component.

potassium binoxalate

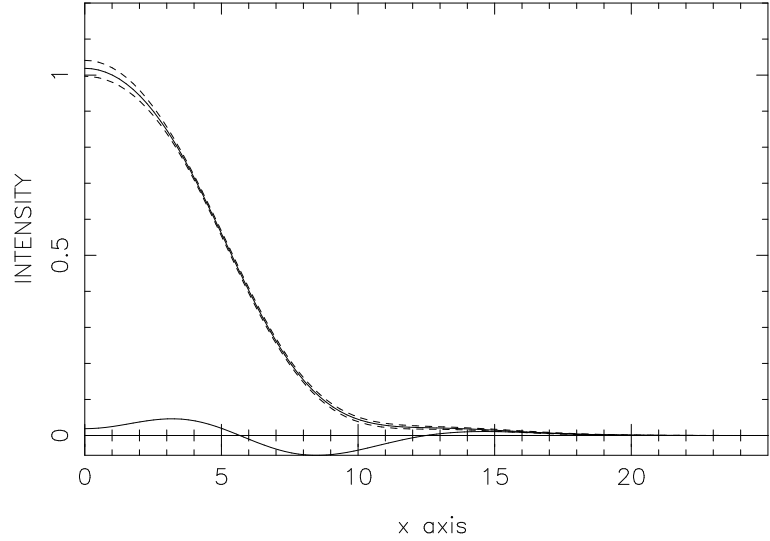


FIG. 7. Momentum distribution for potassium binoxalate along the axis shown. The momentum is in units of \AA^{-1} , $n(\vec{p})$ is in arbitrary units. The errors are calculated as in Eq.(15) for the parameters that are significant in Tables 2 and 3. The lower curve is the anharmonic component.

potassium binoxalate

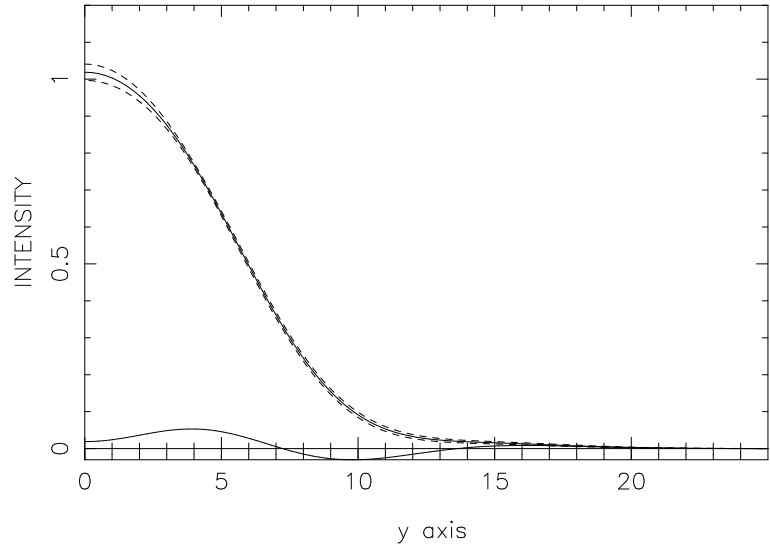


FIG. 8. Momentum distribution for potassium binoxalate along the axis shown. The momentum is in units of \AA^{-1} , $n(\vec{p})$ is in arbitrary units. The errors are calculated as in Eq.(15) for the parameters that are significant in Tables 2 and 3. The lower curve is the anharmonic contribution.

oxalic acid

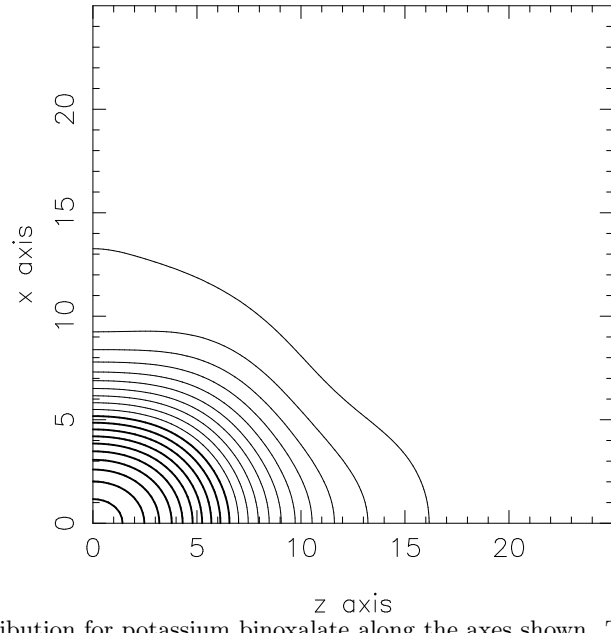


FIG. 9. Momentum distribution for potassium binoxalate along the axes shown. The momentum is in units of \AA^{-1} , $n(\vec{p})$ is in arbitrary units.

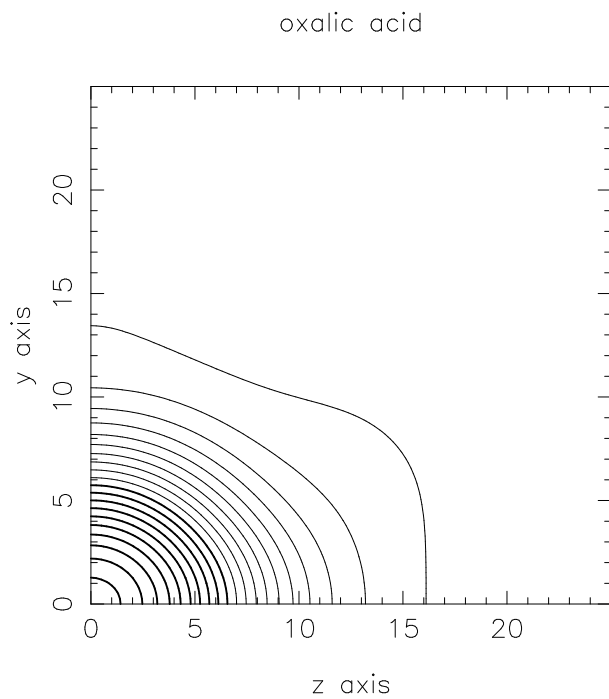


FIG. 10. Momentum distribution for potassium binoxalate along the axes shown. The momentum is in units of \AA^{-1} .

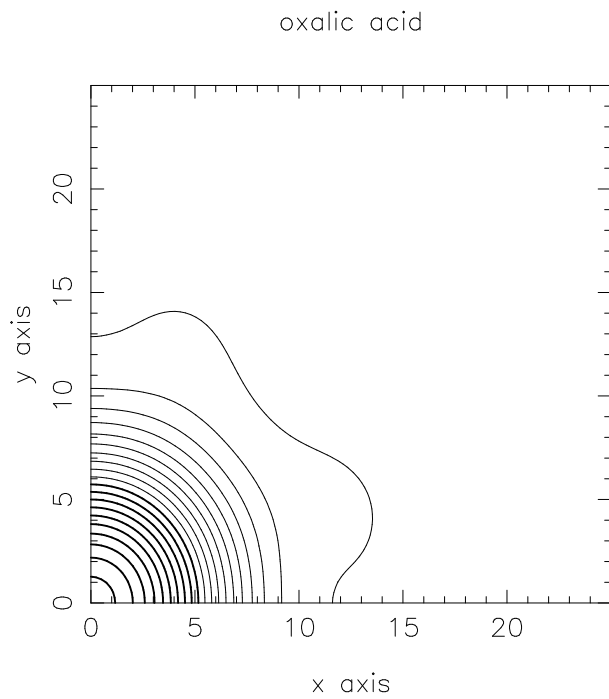


FIG. 11. Momentum distribution for potassium binoxalate along the axes shown. The momentum is in units of \AA^{-1} .

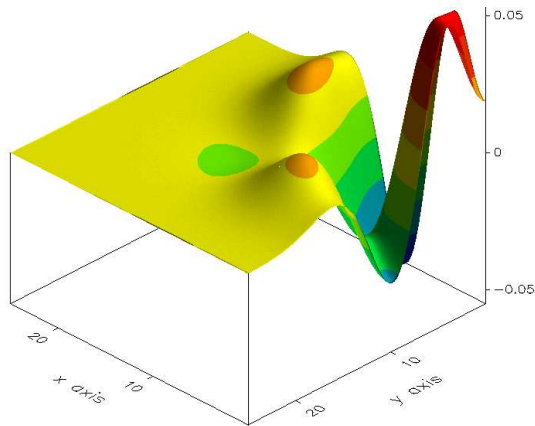


FIG. 12. Anharmonic contribution to the momentum distribution for potassium binoxalate along the axes shown. The momentum is in units of \AA^{-1} .

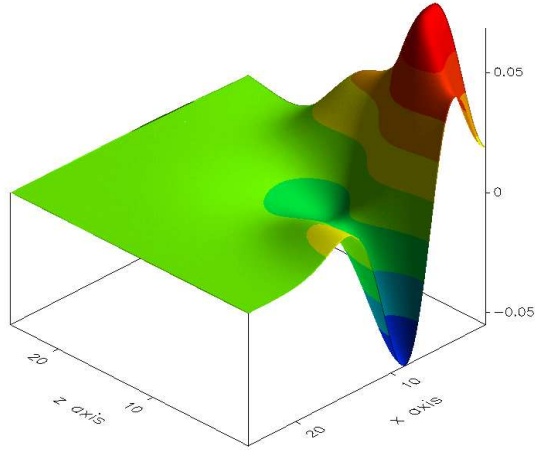


FIG. 13. Anharmonic contribution to the momentum distribution for potassium binoxalate along the axes shown. The momentum is in units of \AA^{-1} .

The coefficients that were measured are given in the tables below.

Table 2. The harmonic fitting coefficients and the variances in their values as measured

Harmonic Coefficients		
i	σ_i	$\delta\sigma_i$
x	4.509	.0235
y	4.869	.0254
z	5.351	.0449

Table 3. The anharmonic fitting coefficients and their variances as measured.

Anharmonic Coefficients				
n	l	m	$a'_{n,l,m}$	$\delta a'_{n,l,m}$
2	0	0	0.0000	0 .0000
1	2	0	-0.1443	0.0377
1	2	2	0.0000	0.0000
0	4	0	0.0510	0.0086
0	4	2	-0.0564	0.0095
0	4	4	0.0000	0.0000
3	0	0	-0.1356	0.0098
2	2	0	-0.0296	0.0105
2	2	2	0.0000	0.0000
1	4	0	-0.000	0.0000
1	4	2	0.0000	0.0000
1	4	4	0.0000	0.0000
0	6	0	-0.0184	0.0065
0	6	2	-0.0127	0.0028
0	6	4	-0.0388	0.0129
0	6	6	0.0000	0.0000
4	0	0	-0.0290	0.0029
3	2	0	0.0000	0.0000
3	2	2	0.0000	0.0000
2	4	0	-0.0016	0.0013
2	4	2	0.0069	0.0013
2	4	4	0.0000	0.0000
1	6	0	-0.0049	0.0021
1	6	2	0.0000	0.0000
1	6	4	-0.0098	0.0036
1	6	6	0.0000	0.0000
0	8	0	0.0000	0.0000
0	8	2	0.0000	0.0000
0	8	4	0.0000	0.0000
0	8	6	0.0000	0.0000
0	8	8	-0.0075	0.0028

Note that there are 14 anharmonic coefficients that are measureable, 13 of which are at the 2σ level at least, and that the harmonic coefficients are measured to better than 1%.

VI. CONCLUSION

We have shown how the method of analysis of DINS data suggested in [10] can be extended to anisotropic momentum distributions, and have applied this method to an analysis of the hydrogen bond in potassium binoxalate. The results

demonstrate that DINS, as it is implemented now at ISIS, is capable of detailed, model independent, measurement of the momentum distribution for hydrogen, and by inference, other light atoms. These measurements required about four days of beam time, and are the first such measurements to be analyzed in this way. The count rates, resolution and detector efficiency can be, and are scheduled to be, significantly improved. The data can be analyzed in less than a day. The DINS technique thus provides a practical means of accessing precise information about the anharmonicity of local potentials and can provide a check of any theoretical calculation of these potentials at a level of accuracy and detail that has not been possible previously.

VII. ACKNOWLEDGEMENTS

We would like to thank Devinder Sivia for assistance in analyzing the data, Steve Bennington and John Tomkinson for useful discussions, and Professors R.G.Delaplane and H. Kuppers for providing the crystals.

APPENDIX A: SEPERABLE DISTRIBUTIONS

The distribution used for the simulations described here is a special case of a general separable distribution

$$n(\vec{p}) = \prod_i n_i(p_i) \quad (A1)$$

If we represent

$$n_i(p_i) = \frac{e^{\frac{-p_i^2}{2\sigma_i^2}}}{(2\pi\sigma_i)^{\frac{1}{2}}} \sum_n a_{i,n} H_n\left(\frac{p_i}{\sqrt{2}\sigma_i}\right) \quad (A2)$$

make use of the fact that

$$\int e^{iqx-x^2} H_n(x) dx = \pi^{\frac{1}{2}} e^{\frac{-q^2}{4}} (iq)^n, \quad (A3)$$

and represent the delta function in the definition of the radon transform by its fourier transform, it is straightforward to show that the Radon transform of $n(\vec{p})$ in the isotropic coordinate system defined in the text is given by

$$J'(\hat{q}', y') = \frac{e^{-y'^2}}{\pi^{\frac{1}{2}}} \sum_{n_j} \left(\prod_i a_{i,n_j} \left(\frac{q'_i}{q'} \right)^{n_j} \right) H_{n_1+n_2+n_3}(y') \quad (A4)$$

For the case we have used as a simulation, in which the distribution is anharmonic only in the z direction, the result simplifies to

$$J'(\hat{q}', y') = \frac{e^{-y'^2}}{\pi^{\frac{1}{2}}} \sum_n (a_{3,n} \cos(\theta')^n) H_n(y') \quad (A5)$$

In this case, the coefficients in the expansion of $J'(\hat{q}', y')$ in the form given by Eq.(3) are not all independent. There is only one independent coefficient in the set of $a_{n,l,0}$ for each value of $2n+l$.

- [1] P. M. Platzmann in 'Momentum Distributions', ed R. N. Silver and P. E. Sokol (Plenum Press, New York, 1989, p249)
- [2] I. Sick in ref 1, page 175.
- [3] R. S. Holt, J. Mayers and A. D. Taylor in ref 1, p. 295
- [4] H. Rauh and N. Watanabe, Phys. Lett. 100A, 244 (1984)
- [5] M. P. Paoli and R. S. Holt, J. Phys. C 21, 3633 (1988)

- [6] S. Ikeda, K. Shibata, Y. Nakai and P. W. Stephens, J. Phys. Soc. Japan 61,2619 (1992)
- [7] P. Postorino, F. Filliaux, J. Mayers, J. Tomkinson and R.S. Holt, J. Chem. Phys. 94, 4411 (1992)
- [8] A L Fielding, D N Timms and J Mayers Europhys. Lett. 44 255 (1998)
- [9] J. Mayers, Phys. Rev. Letts. 71, 1553, (1993)
- [10] R. Silver and G. reiter, Phys. Rev. Letts. **54**, 1047, (1985)
- [11] R. Newton, 'Scattering Theory of Waves and Particles', (Springer, Berlin, 1981)
- [12] V. F. Sears Phys. Rev. B 30, 44 (1984)
- [13] J. Mayers Phys. Rev. B 41, 41 (1991)
- [14] S. W. Lovesey, 'Theory of Neutron Scattering from Condensed Matter', (Oxford University Press, New York, 1987)
- [15] R. Hempelmann, D. Richter and D. L. Price Phys. Rev. Lett. 58, 1016
- [16] M. Warner, S. W. Lovesey and J. Smith Z. Phys. B 39, 2022 (1989)
- [17] This assumes that the temperature is sufficiently low that the proton is essentially in its ground state. This condition is well satisfied for the experiments we will discuss.
- [18] J. Mayers and A. C. Evans, Rutherford Laboratory Report, RAL-91-048 (1991)
- [19] P A Seeger, A D Taylor and R M Brugger Nuc Inst Meth A240 98 (1985)
- [20] V. F. Sears Phys Rev 185 200, (1969), Phys Rev A7 340 (1973)
- [21] D. Sivia, 'Data Analysis: A Bayesian Tutorial', Clarendon Press, Oxford (1996)
- [22] H. Einspahr, R.E. Marsh and J. Donohue, Acta. Cryst. **B28**, 2194, (1972)
- [23] This choice differs from the choice in the previous reference, and corresponds to choice 3 for the unit cell of crystal type 14 with the b axis the unique axis in the standard tables, International Tables for Crystallography, Vol. A, P 177, D. Riedel, (1983),